Dalton Transactions

Accepted Manuscript

ROYAL SOCIETY OF CHEMISTRY

www.rsc.org/dalton

Journal Name

ARTICLE

Nitroxyl as a Ligand in Ruthenium Tetraammine Systems: a Density Functional Theory Study.

Received 00th January 20xx,
Accepted 00th January 20xx

DOI: 10.1039/x0xx00000x

www.rsc.org/

Augusto C. H. Da Silva[a], Juarez L. F. Da Silva[a], Douglas W. Franco[a]*

The properties of the free nitroxyl molecule and the nitroxyl ligand in Ru(II) tetraammines (*trans*-$[Ru(NH_3)_4(nitroxyl)^n(L)]^{2+n}$ (n = nitroxyl charge; L = NH_3, py, $P(OEt)_3$, H_2O, Cl^- and Br^-) were studied using density functional theory. According to the calculated conformational energies, HNO complexes are more stable than their deprotonated analogues, and the singlet configuration (*trans*-$^1[Ru(NH_3)_4(L)HNO]^{2+}$) is lower in energy than the corresponding triplet (*trans*-$^3[Ru(NH_3)_4(L)HNO]^{2+}$). Evaluation of the σ and π components of the L-Ru-HNO bond suggest that the increased stability of these orbitals and the enhanced contributions from the HNO orbitals correlate to shorter Ru-N(H)O distances and higher $\nu_{Ru\text{-}HNO}$ stretching frequencies. The stability of the Ru-HNO bond was also evaluated through a theoretical kinetic study of HNO dissociation from *trans*-$^1[Ru(NH_3)_4(L)HNO]^{2+}$. The order of the Ru-HNO bonding stability in *trans*-$^1[Ru(NH_3)_4(L)HNO]^{2+}$ as a function of L was found to be as follows: H_2O > Cl^- ~ Br^- > NH_3 > py > $P(OEt)_3$. This order parallels the order of the trans-effect and trans-influence series experimentally measured for L in octahedral complexes. The same trend was also observed using an explicit solvent model, considering the presence of both HNO and H_2O molecules in the transition state. For this series, the calculated bond disociation enthalpy for the Ru-HNO bond are in the range 23.8 to 45.7 kcal mol^{-1}. Good agreement was observed between the calculated $\Delta G^{\ddagger}$ values for the displacement of HNO by H_2O in *trans*-$^1[Ru(NH_3)_4(P(OEt)_3HNO]^{2+}$ (23.4 kcal mol^{-1}) and the available experimental data for substitution reactions of trans$[Ru(NH_3)_4(POEt)_3(L_x)]^{2+}$ (19.4 to 24.0 kcal mol^{-1} for L_x = isn and $P(OET)_3$, respectively).

Introduction

HNO (nitroxyl) has attracted the attention of researchers due to its capacities as a pharmacological regulator in processes such as vessel relaxation, as a protective factor during myocardial infarctions, and as an antioxidant, as well as its known protective effects against cancer and use in enabling protein modifications [1–5]. The properties of HNO in physiological media are generally considered to be distinct from those of nitric oxide ($NO^{\cdot}$)[1–5].

The HNO donors exhibit a number of drawbacks, including the release of HNO only at pH values higher than physiological pH, the formation of toxic adducts and the occurrence of parallel reactions. These unwanted effects would restrict, or even preclude, their use in biological systems [1,6–12]. Because the pK_a of ^{1}HNO is approximately 11.4, nitroxyl is present in its protonated form in physiological media [12,13]. In aqueous solution, dimerization reactions lead to the formation of N_2O [5,13–15]; therefore, there is a need for more robust HNO donor systems capable of controlled *in situ* release of HNO in physiological media without the concomitant production of unwanted by-products.

Metal complexes with low-spin d^6 configurations (Fe^{II}, Ru^{II} and Os^{II}), in particular, ruthenium tetraammines [16–19], are interesting options as NO carriers. The two-electron reduction of the formal nitrosonium (NO^+) ligand [20,21] on such compounds (Scheme 1) has the capacity to provide promising options for HNO donors.

Scheme 1: Two electron reduction pathway to coordinated nitrosonium in ruthenium tetraammines.

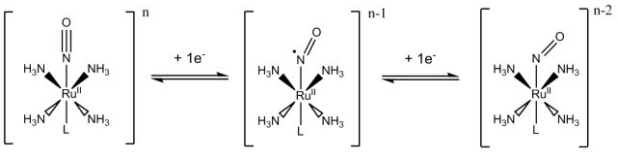

Due to the presence of ammine ligands in the equatorial plane (x⊥y), these compounds are generally water soluble. Furthermore, because ammine ligands are inert to substitution [16,22–24] and to the action of moderate redox [25] reagents, the reactivity of these complexes would be primarily confined along the z-axis. Therefore, the reactivity of the nitrosyl ligand in these ruthenium tetraammines compounds may be tailored [17,23] through judicious selection of the *trans* ligand L. Furthermore, these complexes can act as a NO donors because the reduction of the nitrosonium ligand can be chemically or photochemically induced [16,26]. Several studies report that such compounds may also serve as nitroxyl carriers or donors [20,21,27–30].

Due to the synthetic difficulties associated with nitroxyl complexes and the inherent limitations that these difficulties pose for obtaining experimental data, density functional theory DFT calculations were used to analyze an array of

[a] Instituto de Química de São Carlos, Universidade de São Paulo, Av. Trab. São-Carlense 400, São Carlos, SP, Brazil
E-mail: douglas@iqsc.usp.br

Electronic Supplementary Information (ESI) available: [details of any supplementary information available should be included here]. See DOI: 10.1039/x0xx00000x

nitroxyl metal-porphyrins complexes of d^6 metals (Mn^{I}, Fe^{II}, Co^{III}, Tc^{I}, Ru^{II}, Rh^{III}, Re^{I}, Os^{II}, and Ir^{I}) [14,31] . In all of these systems, despite the isoelectronic nature of the metal centers, there are substantial differences in the formal oxidation state of the metal ions and in the composition of the coordination sphere. This greatly complicates, or even precludes, systematic comparisons between the data sets and correlations with other systems.

Aiming to contribute to the understanding of the descriptive chemistry of HNO as a ligand, this work describes the molecular orbitals and interactions in a set of *trans*-$[Ru(NH_3)_4(L)HNO]^{2+}$ species and related complex ions. The *trans* ligands (L) chosen for comparison were ammine (NH_3) as a ligand with character pure σ, pyridine (py) as a π acceptor ligand, triethyl phosphite ($P(OEt)_3$) as a biphilic ligand, water (H_2O) as a weak π donor ligand, chloride ion (Cl^-) and bromide ion (Br^-) as moderate π and σ donors [19,32–35]. These σ and π ligand characteristics where based in accumulate experience on the ruthenium amine chemistry kinetic and thermodynamic reactivities [19,22,32–36]. This selected group of ligands exhibit different characteristics in terms of the possible molecular orbital combinations and consequently different relative strengths of their trans-influences and trans-effects.

The trans ligand can affect the Ru-HNO bond in two aspects: thermodynamically weakening the Ru-HNO bond (trans influence) and kinetically by labilizing the HNO ligand on respect to substitution (trans effect) [19,36]. The trans influence is related to the differences in energy between the reagents and products (ΔG_{rel}) and therefore experimentally evaluated through the Ru-HNO bond distance, redox potentials and equilibrium formation constants of the *trans*-$[Ru(NH_3)_4L(H_2O)]^{2+}$ from *trans*-$[Ru(NH_3)_4L(HNO)]^{2+}$. The trans effect is correlated to the differences in energy between the reagents and the transition state ($\Delta G_1^{\ddagger}$) and experimentally correlated to the kinetic rate constant (k_1) for L dissociation [19]. Conversely from planar complexes, for octahedral complexes, are very much similar the trans effect and trans influence series for a considerable number of ligands [19,22].

To enable a discussion of the physical characteristics of these species, such as their molecular orbital energies and compositions [37,38], spin variations and reaction energetics, an evaluation of the reaction barriers and reaction mechanism was undertaken, taking advantage of the accumulated experience in the *trans*-$[Ru(NH_3)_4(L)NO]^{3+}$/*trans*-$[Ru(NH_3)_4(L)NO]^{2+}$ systems [16,17,20,21].

Methodology

Ruthenium-nitroxyl interactions in ruthenium tetraammines, such as *trans*-$[Ru(NH_3)_4(L)(nitroxyl)^n]^{2+n}$, were studied using molecular orbital population analyses [39] and considering NBO3 and NBO6 [40] methodologies. The ruthenium-nitroxyl bond dissociation enthalpies were obtained for a series of complexes with different *trans* ligands. The properties of free and coordinated nitroxyl were studied, taking into account their four possible configurations: singlet state anion ($^1NO^{-1}$), triplet state anion ($^3NO^{-1}$), triplet state protonated (^3HNO), and singlet state acid (^1HNO). HNO release was modeled using potential energy surface scanning, and the transition states were obtained using the QST3 [41] method. Furthermore, vibrational analyses were performed in every case to confirm the local minimum configurations (without imaginary frequencies) and the transition states (showing a single imaginary frequency consistent with the HNO release displacement) [41]. The IRC [42] method was also used to confirm the transition states structures in the *trans*-$[Ru(NH_3)_5(HNO)]^{2+}$ system. Since this compound is the simplest one of the series here studied it was selected as a model assuming that similar behavior would be followed by the others related compounds.

In these calculations, the implicit water solvation effects were considered and simulated using the Integral Equation Formalism for the Polarizable Continuum Model (IEFPCM) [43].

The spin-polarized total energy calculations are based on DFT [44,45] within the hybrid B3LYP [46,47] exchange-correlation functional as implemented in the Gaussian03 [48] package. The core and valence electrons are described by DGDZVP [49,50] Gaussian-type orbitals, which include the following: *1s* and *2s* basis functions for H ([2]); *1s*, *2s*, *3s*, *2p*, *3p*, *3d* functions for O, N, and C ([3/2/1]); *1s*, *2s*, *3s*, *4s*, *2p*, *3p*, *4p*, *3d* functions for Cl and P ([4/3/1]); *1s*, *2s*, *3s*, *4s*, *5s*, *2p*, *3p*, *4p*, *5p*, *3d*, 4d functions for Br ([5/4/2]); *1s*, *2s*, *3s*, *4s*, *5s*, *6s*, *2p*, *3p*, *4p*, *5p*, *6p*, *3d*, 4d, *5d 6d* functions for Br ([6/5/3]). To obtain reliable structures, we optimized the atomic forces up to 4.5×10^{-4} with a total energy convergence of 10^{-12} (atomic units, Gaussian default).

Results and Discussion

Free nitroxyl: spin, vibrational and molecular orbital analyses.

The ordering and symmetry of the valence molecular orbitals (M.Os.) for free nitrosonium, nitrosyl and nitroxyl systems in the gas phase were obtained (Figure S1 and Table S1, at Supplementary Information). As a primary observation, the protonated species were found to be energetically more favorable than the deprotonated analogues by at least 30 kcal mol^{-1} [1].

As expected, due to the π and π* M.O. symmetry in diatomic systems, the electronic pairing energies increased the total energy of the singlet systems in the anionic species ($^xNO^-$), resulting in triplet systems $^3NO^-$ ~33 kcal mol^{-1} lower in energy than $^1NO^-$. The addition of a proton breaks the symmetry of the π and π* M.Os., promoting a gap in their respective energy levels and making ^1HNO ~10 kcal mol^{-1} more stable than ^3HNO.

The coordination aspects of the nitroxyl molecule.

Calculations were performed on systems with nitroxyl coordinated to ruthenium(II) tetraammine species (trans-$Ru(NH_3)_4(nitroxyl)^n(L)]^{2+n}$ with L = amine (NH_3), pyridine (py), triethyl phosphite ($P(OEt)_3$), water (H_2O), chloride ion (Cl^-) and bromide ion (Br^-)). For this purpose, the energies and orbital compositions of the four configurations ($^1NO^-$, $^3NO^-$, ^1HNO and ^3HNO) coordinated to the metal center were calculated (Table S2). For all the analyzed complexes, the singlet protonated species were more stable; therefore, only the $[Ru(NH_3)_4(HNO)(L)]^{2+}$ systems were considered further.

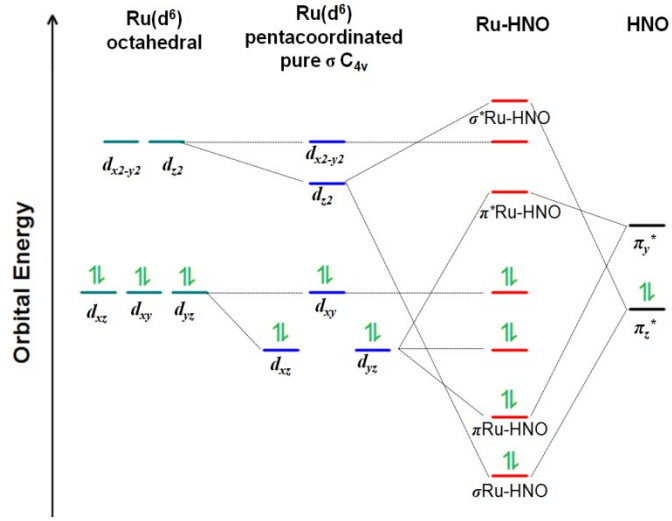

Figure 1: Schematic molecular orbital layout of *d* block orbitals perturbation; including the octahedral Ru(II) d^6 molecular orbital, the ML_5 square pyramidal profiles, and the Ru-HNO molecular orbital interactions in *trans*-$^1[Ru(NH_3)_4(L)HNO]^{2+}$.

The calculations performed using NBO3 and NBO6 methods, (Table S3) exhibit the tendency to neglect the π interactions for all the systems but the py compound and therefore have not been persuaded further.

The M.O. populations and their respective symmetries [37,38] suggest that Ru-HNO interactions are of mainly two types. The first is a σ symmetry interaction, which is the result of a bonding and antibonding combination (σ Ru-HNO and σ^* Ru-HNO, respectively) of the Ru d_{z^2} with the π^*_z orbital of the HNO molecule. The other is a π interaction, which is a consequence of the bonding and antibonding combination (π Ru-HNO and π^* Ru-HNO, respectively) of the Ru d_{xz} orbital with the π^*_x orbital of the HNO molecule (Figure 1). The $^1[Ru(NH_3)_5HNO]^{2+}$ complex shows a coordination sphere of pure σ character with regard to the NH_3 ligands, which, among all the six selected species, most closely resembles the diagram in Figure 1. Therefore, it was taken as a reference for the following discussion. The qualitative M.O. distribution can be visualized trough the molecular orbital isosurfaces, illustrated for $^1[Ru(NH_3)_5HNO]^{2+}$ and *trans*-$^1[Ru(NH_3)_4(P(OEt)_3)HNO]^{2+}$ species in the Figure S2 (S.I.).

The ruthenium d_{z^2} orbital interacts simultaneously with NH_3 and HNO along the octahedral z-axis, forming σ interactions with both ligands. In this complex, this σ ligand orbital (σ Ru-HNO) corresponds to the HOMO-3, and its antibonding orbital (σ^* Ru-HNO) is the LUMO+2. The π component of the Ru-HNO interaction (π Ru-HNO) is observed as the HOMO-2 orbital, and the respective antibonding orbital (π^* Ru-HNO) is the LUMO. The fragment participation of the molecular orbital compositions, as well as the molecular orbitals energies for all the six systems, are described in Table 1.

Trans-$^1[Ru(NH_3)_4(H_2O)HNO]^{2+}$ exhibits the same M.O. sequence as $^1[Ru(NH_3)_5HNO]^{2+}$. The difference between the two is an energetic stabilization, although modest, of all the bonding molecular orbitals, as well a greater involvement of the HNO fragment in the σ Ru-HNO and π Ru-HNO bonding components.

Table 1: Molecular orbital energies (eV) and fragment compositions (%) for the main Ru-nitroxyl interactions.

Species	σ Ru-HNO	π Ru-HNO	π* Ru-HNO	σ* Ru-HNO
$^1[Ru(NH_3)_5HNO]^{2+}$	HOMO-3 (-7.90 eV) (9% dz^2 Ru; 2% $NH_{3(eq)}$; 7% p_z $NH_{3(ax)}$; 81% π_z^*HNO)	HOMO-2 (-7.30 eV) (74% *dzy* Ru; <1% p_y NH_3; 22% π_y^* HNO)	LUMO (-3.23 eV) (30% dzy Ru; <1% $2p_y$ NH_3; 66% π_y^*HNO)	LUMO+2 (-0.63 eV) (60% dz^2Ru; 20% $NH_{3(eq)}$; 5% p_z $NH_{3(ax)}$; 15% π_z^*HNO)
***trans*-$^1[Ru(NH_3)_4(py)HNO]^{2+}$**	HOMO-3 (-8.00 eV) (8% dz^2Ru; 12% p_z N-py; 78% π_z^*HNO)	HOMO-2 (-7.45 eV) (73% *dzy*Ru; 3% $n\pi_y^*$ py; 21% π_y^*HNO)	LUMO (-3.74 eV) (28% dz^2Ru; 2% p_z N-py; 67% π_z^*HNO)	LUMO+4 (-0.76 eV) (61% *dzy*Ru; 8% $n\pi_y^*$ py; 16% π_y^*HNO)
***trans*-$^1[Ru(NH_3)_4(P(OEt)_3)HNO]^{2+}$**	HOMO-3 (-7.72 eV) (7% dz^2Ru; 39% n*p* $P(OEt)_3$; 53% π_z^*HNO)	HOMO-2 (-7.02 eV) (73% *dzy*Ru; 3% n*p* $P(OEt)_3$; 18% π_y^*HNO)	LUMO (-3.37 eV) (24% *dzy*Ru; 4% n*p* $P(OEt)_3$; 70% π_y^*HNO)	LUMO+1 (-0.85 eV) (58% dz^2Ru; 15% n*p* $P(OEt)_3$; 11% π_z^*HNO)
***trans*-$^1[Ru(NH_3)_4(H_2O)HNO]^{2+}$**	HOMO-3 (-8.12 eV) (12% dz^2Ru; 3% p_z H_2O; 83% π_z^*HNO)	HOMO-2 (-7.46 eV) (71% *dzy*Ru; 3% 2*py* H_2O; 23% π_y^*HNO)	LUMO (-3.28 eV) (31% dz^2Ru; 4% p_z H_2O; 65% π_z^*HNO)	LUMO+2 (-1.06 eV) (59% *dzy*Ru; 13% 2*py* H_2O; 20% π_y^*HNO)
***trans*-$^1[Ru(NH_3)_4(Cl)HNO]^{1+}$**	HOMO-3 (-7.47 eV) (6% dz^2Ru; 26% p_z Cl^-; 66% π_z^*HNO)	HOMO-2 (-6.79 eV) (51% *dzy*Ru; 25% 2*py* Cl^-; 21% π_y^*HNO)	LUMO (-2.93 eV) (33% dz^2Ru; 4% p_z Cl^-; 62% π_z^*HNO)	LUMO+2 (-0.65 eV) (60% *dzy*Ru; 7% 2*py* Cl^-; 17% π_y^*HNO)
***trans*-$^1[Ru(NH_3)_4(Br)HNO]^{1+}$**	HOMO-3 (-7.36 eV) (7% dz^2Ru; 44% p_z Br^-; 46% π_z^*HNO)	HOMO-1 (-6.69 eV) (54% *dzy*Ru; 11% 2*py* Br^-; 32% π_y^*HNO)	LUMO (-3.00 eV) (32% dz^2Ru; 2% p_z Br^-; 63% π_z^*HNO)	LUMO+2 (-0.82 eV) (59% *dzy*Ru; 9% 2*py* Br^-; 17% π_y^*HNO)

Table 2: Experimental (expt) and calculated (calc) geometric parameters of different nitroxyl complexes and the Ru-HNO bonding stretching frequencies ($\nu_{Ru\text{-}HNO}$) and N-O bonding stretching frequencies of the nitroxyl group (ν_{NO}).

Species		$R_{N\text{-}O}$ (Å)	$R_{Ru\text{-}N(H)O}$ (Å)	A_{HNO} (deg)	$A_{M\text{-}N\text{-}O}$ (deg)	ν_{NO} (cm^{-1})	$\nu_{Ru\text{-}HNO}$ (cm^{-1})	*ref*
^{1}HNO	expt	1.212	-	108.6	-	1563		51–53
	calc	1.214	-	108.1	-	1668		a
Ru(TTP)(HNO)(1-MeIm)	expt					1380		54
	calc	1.248	1.940	112.0	132.1	1382		54
Ru(HNO)('$py^{bu}S_4$')	expt	1.242	1.875		130.0	1358		55
	calc	1.250	1.953	111.7	130.7	1370		55
$Mb^{II}HNO$	expt	1.240	1.820		131.0	1385		56
$^1[Fe(CN)_5HNO]^{3-}$	expt					1380		27
$[Os(Cl)_2(CO)(HNO)(PPh_3)_2]^{2+}$	expt	1.193	1.915	99.0	136.9	1410		57
$^1[Ru(NH_3)_5(HNO)]^{2+}$	calc	1.244	1.916	111.3	127.6	1478	685	a
trans-$^1[Ru(NH_3)_4(py)(HNO)]^{2+}$	calc	1.242	1.925	110.9	126.7	1489	649	a
trans-$^1[Ru(NH_3)_4(P(OEt)_3)(HNO)]^{2+}$	calc	1.237	1.974	111.0	127.1	1509	600	a
trans-$^1[Ru(NH_3)_4(H_2O)(HNO)]^{2+}$	calc	1.242	1.888	111.9	127.9	1481	680	a
trans-$^1[Ru(NH_3)_4(Cl)(HNO)]^{1+}$	calc	1.249	1.903	111.3	127.8	1456	647	a
trans-$^1[Ru(NH_3)_4(Br)(HNO)]^{1+}$	calc	1.248	1.906	111.4	127.7	1459	640	a

[a] DFT B3LYP/DGDZVP with IEFPCM used at this work.

In the *trans*-$^1[Ru(NH_3)_4(Cl)HNO]^{1+}$ system, the order described above is maintained; however, both the energy stabilization and the participation of the HNO orbitals in the σ and π components are smaller than in the $^1[Ru(NH_3)_5HNO]^{2+}$ system (see Table 1). For the *trans*-$^1[Ru(NH_3)_4(Br)HNO]^1$ ion, the σ and π Ru-HNO interactions are observed in the HOMO-3 and HOMO-1, respectively. The π^* Ru-HNO and σ^* Ru-HNO antibonding interactions occur in the LUMO and LUMO+2, respectively.

The small stabilization in energy of the π Ru-HNO component in this system as compared to $^1[Ru(NH_3)_5HNO]^{2+}$ accounts for the difference in orbital order in the *trans*-bromide complex.

For the *trans*-$^1[Ru(NH_3)_4(py)HNO]^{2+}$ system, the σ and π bonding components are observed as the HOMO-3 and HOMO-2, respectively. The antibonding π^* and σ^* components are observed as the LUMO and LUMO+4, respectively. The n_π^* orbitals of the pyridine ring, which exhibit energies similar to the π^* and σ^* of the Ru-HNO system, are likely the cause the change in the orbital order from that shown in Figure 1. A comparison of the orbital energies indicates that the σ Ru-HNO and π Ru-HNO interactions in the pyridine complex lead to a ~0.1 eV stabilization as compared with the $^1[Ru(NH_3)_5HNO]^{2+}$ system. Nevertheless, the participation of the HNO orbitals in the bonding is slightly smaller (see Table 1).

In the *trans*-$^1[Ru(NH_3)_4(P(OEt)_3)HNO]^{2+}$ complex, the bonding σ Ru-HNO and π Ru-HNO interactions occur in the HOMO-3 and HOMO-2, respectively, and the antibonding π^* Ru-HNO and σ^* Ru-HNO interactions as the LUMO and LUMO+1, respectively. A 0.23 eV destabilization is observed between the bonding orbitals, with the consequent stabilization of the antibonding orbitals. This is in line with the lower participation of the HNO orbitals in these components relative to the interactions in $^1[Ru(NH_3)_5HNO]^{2+}$ (Table 1).

Table 2 lists the calculated and available experimentally measured bond distances and angles in HNO and the Ru-N(H)O fragments for selected species. Very good agreement was observed between the experimental and calculated data [27,55-61] for $R_{N\text{-}O}$ and $A_{H\text{-}N\text{-}O}$ in HNO using B3LYP/DGDZVP. However, this basis set overestimates the ν_{NO} by a factor of 1.07 [58]. Taking this correction into account, all of the calculated ν_{NO} values for the ruthenium ammine species would be in the 1381-1410 cm^{-1} (L= NH_3 and $P(OEt)_3$) range, consistent with the experimental values found for other compounds. The variations in the Ru-HNO bond lengths (Ru-N(H)O, see Table 2), and therefore in the Ru-HNO stretching frequencies ($\nu_{Ru\text{-}HNO}$), are manifestations of the so called trans influence, which is thermodynamic in nature and would express the weakening of the Ru-NHO bond as consequence of the trans ligand L [32,59]. The variations in energies and in the compositions of the molecular orbitals comprising the σ Ru-HNO and π Ru-HNO bonds are induced by the nature of the trans ligand (L), which will compete for the σ and π bond components of the Ru-HNO interactions (see Table 1).

The $^1[Ru(NH_3)_5HNO]^{2+}$ and *trans*-$^1[Ru(NH_3)_4(H_2O)HNO]^{2+}$ systems are not very much different in these terms. The Ru-HNO bond lengths ($R_{Ru\text{-}N(H)O}$) are 1.916 Å and 1.888 Å, the $\nu_{Ru\text{-}HNO}$ stretching values are 685 cm^{-1} and 680 cm^{-1}, the higher values in the studied series, for the pentaammine and the *trans*-aquotetraammine species, respectively, (See Table 2). In the *trans*-$^1[Ru(NH_3)_4(P(OEt)_3)(HNO)]^{2+}$ system, the smaller stabilization of the σ and π Ru-HNO bond components and the smaller contributions from the π^* HNO fragment orbitals

would account for the Ru-N(H)O distance 1.974 Å, the $\nu_{Ru\text{-}HNO}$ stretching value of 600 cm^{-1}. These parameters ($\nu_{Ru\text{-}HNO}$, $R_{Ru\text{-}N(H)O}$) can give us a perspective of the relative stability of the Ru-HNO bond in the series here studied.

However, the simplest bond distances and stretching energies comparison would be just initial analyses to be complemented with the kinetic and thermodynamic study performed ahead.

At this point, nothing could be said about the relative acidity of the HNO ligands in the title complexes based on bond distances $D_{H\text{-}N(HNO)}$ and stretching $\nu_{H\text{-}N(HNO)}$ data (See Table S3 in the supporting information). Considering that the σ component of the $[Ru(NH_3)_4(L)^n]^{n+2}$ → HNO bonding is stronger than the π component, and thus assuming a simplified electrostatic model, higher positive charges on the metal center in the $[Ru(NH_3)_4(L)^n]^{n+2}$ moiety will result in greater polarization of the nitroxyl ligand [60] and enhancements in the acidity of the nitroxyl proton. Therefore, based on the Mulliken charges of the metal centers in the $[Ru(NH_3)_4(L)^n]^{n+2}$ fragments, the following represents the relative order of decreasing pK_a values the proton as a function of L: $P(OEt)_3$ > Cl^- > Br^- > py > H_2O > NH_3.

Because a pK_a value of 9.9 was estimated for *trans*-$^1[Ru(NH_3)_4(P(OEt)_3)(HNO)]^{2+}$ [20], the other compounds should exhibit correspondingly lower pK_a values. This value is suitable, considering that the coordinated HNO pka in another nitroxyl complexes were measured with values = 7.7 [27] and 9.8 [61].

Effects of the trans-ligand on the ruthenium-nitroxyl bond.

Using the BDE method, the energy of the Ru(II)-HNO bond in $^1[Ru(Por)(5\text{-}MeIm)(HNO)]^{2+}$ [14] was calculated to be 24.60 kcal mol^{-1}. Initially, similar calculations were performed for the tetraammines leading to values in the range of 23.76 to 45.68 kcal mol^{-1} (Table 3). The BDE values are obtained through the enthalpy calculation of three different isolated conformations: haxacoordinated species, *trans*-$^1[Ru(NH_3)_4(L)HNO]^{2+}$; pentacoordinated species, $^1[Ru(NH_3)_4(L)]^{2+}$; and free nitroxyl species, ^{1}HNO. All these calculated energies, according to the Equation 1, are show in Table S4.

$$BDE = (\Delta H_{pentacoordinated} + \Delta H\,^1{}_{HNO}) - \Delta H_{hexacoordinated} \quad (1)$$

BDE data are thermodynamic descriptors; however, in dealing with solutions, a kinetic approach would likely be more useful.

To gain insight into how the complex ion fragment *trans*-$[Ru(NH_3)_4(L)]^{2+}$ stabilizes the coordinated HNO molecule, reactions involving the release of nitroxyl (^{1}HNO) were investigated (Figure 2). The calculations were performed with the assumption that ^{1}HNO dissociates preferentially to L= $P(OEt)_3$ and py.

$$trans\text{-}^1[Ru(NH_3)_4(L)(HNO)]^{2+} \rightleftharpoons {}^1[Ru(NH_3)_4(L)]^{2+} + {}^1HNO \quad (2)$$

For these systems, experimental evidence indicates that two-electron reductions of *trans*-$^1[Ru(NH_3)_4(L)NO]^{3+}$ lead to the formation of the aqua species *trans*-$^1[Ru(NH_3)_4(L)H_2O]^{3+}$ and N_2O as the product of fast HNO dimerization [6,15,62] (k_{dim} = 8 x 10^6 s^{-1} M^{-1}), as following summarized:

$$trans\text{-}^1[Ru(NH_3)_4(L)NO]^{3+} + 2e^- \overset{fast}{\rightleftharpoons} trans\text{-}^1[Ru(NH_3)_4(L)NO]^{+} \quad (3)$$

$$trans\text{-}^1[Ru(NH_3)_4(L)NO]^{+} + H^+ \overset{fast}{\rightleftharpoons} trans\text{-}^1[Ru(NH_3)_4(L)(HNO)]^{2+} (4)$$

$$trans\text{-}^1[Ru(NH_3)_4(L)(HNO)]^{2+} + H_2O \overset{slow}{\underset{k_{-HNO}}{\rightleftharpoons}} trans\text{-}^1[Ru(NH_3)_4(L)(H_2O)]^{2+} + {}^1HNO \quad (5)$$

$$2\ {}^1HNO \overset{fast}{\underset{k_{dim}}{\rightleftharpoons}} N_2O + H_2O \quad (6)$$

Based on the accumulated experience with nitrosyl complexes [16,17], it is likely that the others ligands will show similar tendencies, except for L = Cl^- and Br^-. By analogy with observations made for systems where L= $P(OEt)_3$ and $P(OH)(OEt)_2$, where k_{-NO} = 0.98 $s^{-1}M^{-1}$ and 0.24 $s^{-1}M^{-1}$, respectively [20,21], it is likely that the dissociation of HNO (k_{-HNO}, eq. 4) from *trans*-$[Ru(NH_3)_4L(HNO)]^{2+}$ occurs at comparable or higher rates than the dissociation of NO (k_{-NO}) from the *trans*-$[Ru(NH_3)_4L(NO)]^{2+}$ ions. The data for water exchange in *trans*-$[Ru(NH_3)_4L(H_2O)]^{2+}$ are not available in the literature. However, from kinetic studies on substitution reactions of *trans*-$[Ru(NH_3)_4P(OEt)_3(H_2O)]^{2+}$, an upper limit of 10 s^{-1} has been suggested for this reaction [33].

The fast dimerization of ^{1}HNO (8x10^6 M^{-1} s^{-1} [15,62]) is an important factor in shifting the equilibrium in eq. 5 and Figure 3 to the right. As such, it is likely that the rate-determining step is HNO dissociation (k_{-HNO}, eq. 5), which depends strongly on the identity of the trans-ligand L.

The simplest model to examine these bonds was to evaluate the relative energy of the Ru(II)-HNO bond starting from a hexacoordinate *trans*-$^1[Ru(NH_3)_4(HNO)(L)]^{2+}$ system through bond breakage and the formation of a pentacoordinated species ($[Ru(NH_3)_4(L)]^{2+}$) and a free HNO molecule (Eq. 2, Figure 2).

As shown in Figure 2, the calculation route starts with the hexacoordinate complex, from which a scan of the potential energy surface (PES) of the Ru-N(HNO) bond was carried out.

From the PES profile, a new minimum energy conformation can be visualized in which the HNO is outside the coordination sphere of the metal. The following three optimized structures are necessary to describe the reaction pathway: the hexacoordinate structure (reagent complex, RC), the pentacoordinate structure and uncoordinated ^{1}HNO (product complex, PC), and the transition state (TS) structure. The reliability of these structures was checked [58] by calculating the vibrational modes for each system.

Figure 2: General scheme for HNO release reaction through the Ru-NHO bond cleavage.

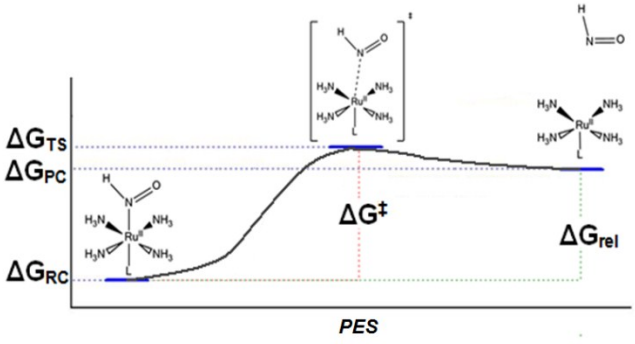

Table 3: [a] Ru(II)-HNO BDE data, HNO release activation barriers ($\Delta G^{\ddagger}$) and respective relative energies for pentacoordinate complexes with free HNO (ΔG_{rel}) in kcal mol^{-1}.

Species	BDE	$\Delta G^{\ddagger}$ (kcal mol^{-1})	ΔG_{rel}
$^1[Ru(NH_3)_5HNO]^{2+}$	39.2	35.6	34.7
trans-$^1[Ru(NH_3)_4(py)HNO]^{2+}$	35.6	31.0	30.9
trans-$^1[Ru(NH_3)_4(P(OEt)_3)HNO]^{2+}$	23.8	21.4	19.2
trans-$^1[Ru(NH_3)_4(H_2O)HNO]^{2+}$	45.7	41.5	41.2
trans-$^1[Ru(NH_3)_4(Cl)HNO]^{1+}$	44.1	38.9	b
trans-$^1[Ru(NH_3)_4(Br)HNO]^{1+}$	42.9	39.4	b

a) Considering the Figure 2 scheme. Uncertainty of ± 0.5 Kcal [48] b) The *trans*-$^1[Ru(NH_3)_4(Cl)HNO]^{1+}$ and *trans*-$^1[Ru(NH_3)_4(Br)HNO]^{1+}$ species, the pentacoordinated with free HNO not a PES minimum.

The minima do not exhibit imaginary frequencies, whereas the saddle point shows one imaginary frequency in which the atomic displacement is compatible with the separation of HNO from the coordination sphere.The activation barrier for HNO dissociation ($\Delta G^{\ddagger}$) and the relative stability of the pentacoordinate complex (ΔG_{rel}) in relation to the hexacoordinate species were calculated (Table 3). According to Figure 2, the activation free energy ($\Delta G^{\ddagger}$) is obtained as the difference in relative energies of the transition state and the hexacoordinate reactant complex ($\Delta G^{\ddagger} = \Delta G_{TS} - \Delta G_{RC}$) [41]. The relative Gibbs free energy for product formation is the difference between the free energies of the product complex and the hexacoordinate reactant complex ($\Delta G_{rel} = \Delta G_{PC} - \Delta G_{RC}$).

The higher the value of $\Delta G^{\ddagger}$ (Table 3), the greater the energy required to remove the HNO from the coordination sphere. The following relative bonding energy sequence was calculated for breaking the Ru-HNO bond in *trans*-$^1[Ru(NH_3)_4(L)HNO]^{2+}$ as function of L: (H_2O) > Br^- ~ Cl^- > (NH_3) > (py) > ($P(OEt)_3$). The same relative order is also observed on basis of both the ΔG_{rel} and BDE values for the Ru-HNO bond (Table 3). This observation would express the trend on the energy necessary to break the Ru-HNO bond. This trend was initially envisaged in the initial analyses of the σ and π bonding components,the Ru-N(H)O atomic distances and $\nu_{Ru\text{-}HNO}$ stretching, see Tables 1 and 2.

This order above follows the same sequence of increasing trans-effect and trans-influence of L, calculated on basis of experimental kinetic and thermodynamic data for octahedral ammine complexes [32,33].

Table 4: Substitution mechanism in nitroxyl ruthenium tetraammines relative energies (in kcal mol^{-1}) for stationary structures of reactant complex (reference, RC), first transition state (TSI), intermediate (INT), second transition state (TSII) and product complex (PC).

Species	RC	TSI	INT	TSII	PC
	(kcal mol^{-1})				
$^1[Ru(NH_3)_5HNO]^{2+}$	0.0	34.2	33.8	36.2	28.8
trans-$^1[Ru(NH_3)_4(H_2O)HNO]^{2+}$	0.0	43.5	41.9	44.5	35.4
trans-$^1[Ru(NH_3)_4(P(OEt)_3)HNO]^{2+}$	0.0	22.4	22.2	23.4	17.3

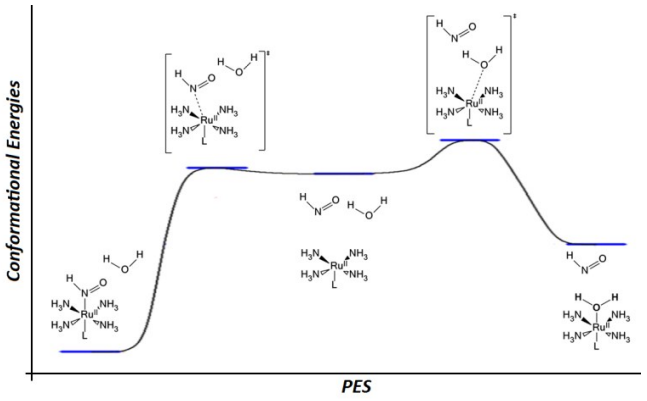

Figure 3: Schematic of the potential energy surface for the nitroxyl substitution reactions.

Conversely from planar complexes, for octahedral complexes, are very much similar the trans effect and trans influence series for a considerable number of ligands [19,22,32] .

To better describe the HNO release (eq. 5), replacement of HNO with a water molecule (from solvent) must be included. Therefore, we included in the matrix calculation a spatially oriented water molecule, facilitating its approach to the metal center where it occupies the site of the departed HNO.

A new PES scan was performed by varying the HNO distance to the metal center and allowing the water molecule to move to find an energetically favorable geometry. Three selected systems have been studied in more detail. These are the *trans*-$^1[Ru(NH_3)_4(H_2O)HNO]^{2+}$ and *trans*-$^1[Ru(NH_3)_4(P(OEt)_3)HNO]^{2+}$ complexes, wherein the Ru-HNO bond is the strongest and weakest in the series, respectively, and $^1[Ru(NH_3)_5HNO]^{2+}$, which is the simplest for computation.

For these three systems, the scan leads to a new minimum (reaction's intermediate (INT)) in which both the nitroxyl molecule and water molecule are uncoordinated (or very weakly bound, or semi-coordinated) to the metal center.

From this new minimum, a second scan was performed by varying the water-ruthenium distance coordinate and allowing the nitroxyl molecule to re-orient to achieve the most energetically favorable conformation. A new minimum is detected in which the exchange of the HNO ligand for water is complete. Therefore, the PES of this replacement has the three following minima (Figure 3): HNO coordinated and water uncoordinated (RCs), both (HNO and water) outside the coordination sphere (INT), and coordinated water with HNO outside the coordination sphere (PCs). These minima are connected by two transition states representing the dissociation of HNO (TSI) and the binding of water (TSII). The conformational energies obtained were normalized with respect to their respective reactant complexes (RC). The relative energies are show in the Table 4.

These results follow the same relative order discussed above (Table 3). However, with the water molecule addiction in the calculation matrix, the activation barriers to the HNO dissociation are similar (1-3 kcal mol^{-1}) in comparison with the same system without the solvent molecule. The complete reaction ΔG values are lowered (4-15 kcal mol^{-1}), that can be explained by the hexacoordinated system restitution.

These results supporting the hypothesis that the ruthenium nitroxyl bond Ru-HNO is very sensitive to the *trans*-ligand effect and influence of L [32,33]. The stronger the trans-effect and trans-influence of *trans*-(L), the weaker the Ru-N(H)O bond will be. It is

noteworthy that the experimental $\Delta G^{\ddagger}$ data [33,59] reported for a series of substitution reactions with the equation 7:

$$trans - [Ru(NH_3)_4(P(OEt)_3)(L_x)]^{3+} + H_2O \rightleftharpoons trans - [Ru(NH_3)_4(P(OEt)_3)(H_2O)]^{3+} + L_x \quad (7)$$

where L_x = CO; $P(OET)_3$, isonicotinamide (isn), pyrazine (Pz) and imidazole (ImN), show $\Delta G^{\ddagger}$ values in the range of 19.4 (Isn) to 24.0 ($P(OET)_3$) kcal mol^{-1}. These are not far from the $\Delta G^{\ddagger}$ value of 22.4 kcal mol^{-1} calculated for HNO dissociation from *trans*-^{1}[$Ru(NH_3)_4(P(OEt)_3)HNO]^{2+}$ (Table 4).

Conclusions

Assuming a neutral aqueous solution, the singlet state of the HNO ligand is more stable than the triplet state in the complexes studied, and it is likely that this tendency would hold for coordination compounds with metals in d^6 low-spin configurations.

The singlet form of *trans*-$[Ru(NH_3)_4(L)(nitroxyl)^n]^{2+n}$ is stabilized with regard to the corresponding triplet by 27.9 ($P(OEt)_3$) to 35.4 (Cl^-) kcal mol^{-1}. High stability of the orbitals responsible for the π and σ bonding components and large the contributions from the HNO orbitals to these components lead to small Ru-N(H)O distances as well as higher values for $\nu_{Ru\text{-}HNO}$ stretching frequencies.

The BDE calculations for the Ru-HNO bond vary in the range of 23.8 (L = $P(OEt)_3$) to 45.7 kcal mol^{-1} (L = H_2O). These same trend was observed considering the kinetic approach trough the transition states determination, where the free energy barrier to the HNO dissociation ($\Delta G^{\ddagger}$) vary from 21.4 (L = $P(OEt)_3$) to 41.5 kcal mol^{-1} (L = H_2O). The HNO substitution reactions by the solvent molecule shows similar free energy activation barriers (23.4 kcal mol^{-1}, L = $P(OEt)_3$, to 44.5 kcal mol^{-1}(L = H_2O)) observed considering a pure dissociative mechanism. However the aquation product complex (*trans*-$[Ru(NH_3)_4(P(OEt)_3)(H_2O)]^{2+}$) is favored regarding to the pentacoordinated ($[Ru(NH_3)_4(P(OEt)_3)]^{2+}$) system through ΔG_{rel} stabilization by at least 4.1 kcal mol^{-1}. The pentacoordinate species are energetically unfavorable with respect to the hexacoordinated species, as expected on account of the known preference of Ru^{II} for hexacoordination. In aqueous media, the leaving group (HNO) is replaced by the solvent (H_2O), forming a new complex and reestablishing hexacoordination.

As could be anticipated based on the accumulated knowledge of ruthenium tetraammines, the Ru(HNO) bond characteristics (Ru-N(H)O) distance, $\nu_{Ru\text{-}HNO}$ stretching) were influenced by the ligand in the position trans to HNO. The same is true regarding the calculated BDE, $\Delta G^{\ddagger}$ and ΔG_{rel} energies (Tables 3 and 4). The energy required to break the Ru-N(H)O bond in *trans*-^{1}[$Ru(NH_3)_4(L)HNO]^{n+}$ decreases as function of L as follows: $P(OEt)_3$ < py < NH_3 < Cl^- < Br^- < H_2O.

The range of $\Delta G^{\ddagger}$ values for the dissociation of HNO from complexes with different *trans*-(L) ligands is a consequence of the electronic distribution in the bonding orbitals along the L-Ru-N(H)O coordinate (Table 1), and their consequent stabilization in comparison to the corresponding anti-bonding orbitals (Table 1). An evenly distributed bonding orbital along the L-Ru-N(H)O axis with a high bonding-antibonding energy gap results in higher $\Delta G^{\ddagger}$ values and a more stable Ru-N(H)O bond.

The calculated free energies barriers to the ligand replacement in the *trans*-^{1}[$Ru(NH_3)_4(P(OEt)_3)HNO]^{2+}$ shows similar values to the ones available in the literature experimental data.

Acknowledgements

The authors acknowledge FAPESP (grant number 2012/222-7) for the financial support.

References

1 J. M. Fukuto, C. H. Switzer, K. M. Miranda and D. a Wink, *Annu. Rev. Pharmacol. Toxicol.*, 2005, **45**, 335–55.
2 J. M. Fukuto, C. L. Bianco and T. a Chavez, *Free Radic. Biol. Med.*, 2009, **47**, 1318–24.
3 T. W. Miller, M. M. Cherney, A. J. Lee, N. E. Francoleon, P. J. Farmer, S. B. King, A. J. Hobbs, K. M. Miranda, J. N. Burstyn and J. M. Fukuto, *J. Biol. Chem.*, 2009, **284**, 21788–96.
4 C. H. Switzer, W. Flores-Santana, D. Mancardi, S. Donzelli, D. Basudhar, L. a Ridnour, K. M. Miranda, J. M. Fukuto, N. Paolocci and D. a Wink, *Biochim. Biophys. Acta*, 2009, **1787**, 835–40.
5 K. M. Miranda, *Coord. Chem. Rev.*, 2005, **249**, 433–455.
6 N. Paolocci, M. I. Jackson, B. E. Lopez, K. Miranda, C. G. Tocchetti, D. a Wink, A. J. Hobbs and J. M. Fukuto, *Pharmacol. Ther.*, 2007, **113**, 442–58.
7 J. C. Irvine, J. L. Favaloro and B. K. Kemp-Harper, *Hypertension*, 2003, **41**, 1301–7.
8 K. M. Miranda, H. T. Nagasawa and J. P. Toscano, *Curr. Top. Med. Chem.*, 2005, 649–664.
9 K. M. Miranda, T. Katori, C. L. T. De Holding, L. Thomas, L. A. Ridnour, W. J. Mclendon, S. M. Cologna, A. S. Dutton, H. C. Champion, D. Mancardi, C. G. Tocchetti, J. E. Saavedra, L. K. Keefer, K. N. Houk, J. M. Fukuto, D. A. Kass, N. Paolocci and D. A. Wink, *J. Med. Chem.*, 2005, **48**, 8220–8228.
10 X. Sha, T. S. Isbell, R. P. Patel, C. S. Day and S. B. King, *J. Am. Chem. Soc.*, 2006, **128**, 9687–9692.
11 Y. Adachi, H. Nakagawa, K. Matsuo, T. Suzuki and N. Miyata, *Chem. Commun. (Camb).*, 2008, 5149–51.
12 M. D. Bartberger, W. Liu, E. Ford, K. M. Miranda, C. Switzer, J. M. Fukuto, P. J. Farmer, D. A. Wink and K. N. Houk, *PNAS*, 2002, **99**, 10958–10963.
13 J. C. Irvine, R. H. Ritchie, J. L. Favaloro, K. L. Andrews, R. E. Widdop and B. K. Kemp-Harper, *Trends Pharmacol. Sci.*, 2008, **29**, 601–8.
14 L. Yang, W. Fang and Y. Zhang, *Chem. Commun. (Camb).*, 2012, **48**, 3842–4.
15 C. Fehling and G. Friedrichs, *J. Am. Chem. Soc.*, 2011, **133**, 17912–17922.
16 E. Tfouni, M. Krieger, B. R. Mcgar and D. W. Franco, *Coord. Chem. Revews*, 2003, **236**, 57–69.
17 E. Tfouni, F. G. Doro, L. E. Figueiredo, J. C. M. Pereira, G. Metzker and D. W. Franco, *Curr. Med. Chem.*, 2010, **17**, 3643–3657.
18 J. F. DuMond and S. B. King, *Antioxid. Redox Signal.*, 2011, **14**, 1637–48.
19 H. Taube, *Comments Inorg. Chem.*, 1981, **1**, 17–31.
20 G. Metzker, E. V. Stefaneli, J. C. M. Pereira, F. D. C. A. Lima, S. C. Da Silva and D. W. Franco, *Inorganica Chim. Acta*, 2013, **394**, 765–769.
21 D. R. Truzzi and D. W. Franco, *Inorganica Chim. Acta*, 2014, **421**, 74–79.
22 S. Isied and H. Taube, *Inorg. Chem.*, 1976, **15**, 3070–3075.
23 P. C. Ford and C. Sutton, *Inorg. Chem.*, 1969, **8**, 1544–1546.
24 H. Taube, *Surv. Prog. Chem.*, 1973, **1**.
25 M. G. Gomes, C. U. Davanzo, S. C. Silva, L. G. F. Lopes, P. S. Santos and D. W. Franco, *J. Chem. Soc. Dalt. Trans.*, 1998, 601–608.
26 B. C. S. Allardyce and P. J. Dyson, *Platin. Met. Rev.*, 2001, **45**, 62–69.

27 A. C. Montenegro, V. T. Amorebieta, L. D. Slep, D. F. Martín, F. Roncaroli, D. H. Murgida, S. E. Bari and J. A. Olabe, *Angew. Chem. Int. Ed. Engl.*, 2009, **48**, 4213–6.
28 M. Sieger, B. Sarkar, S. Záliš, J. Fiedler, N. Escola, F. Doctorovich, A. Olabe and W. Kaim, *Dalt. Trans.*, 2004, 1797–1800.
29 L. E. Goodrich and N. Lehnert, *J. Inorg. Biochem.*, 2013, **118**, 179–86.
30 M. A. Martı, S. E. Bari, A. Estrin and F. Doctorovich, *J. Am. Chem. Soc.*, 2005, **127**, 4680–4684.
31 Y. Zhang, *J. Inorg. Biochem.*, 2013, **118**, 191–200.
32 J. do Nascimento Filho, J. B. de Lima, B. dos S. Lima Neto and D. W. Franco, *J. Mol. Catal.*, 1994, **90**, 257–266.
33 D. Franco and H. Taube, *Inorg. Chem.*, 1978, **17**, 0–7.
34 R. E. Shepherd and H. Taube, *Inorg. Chem.*, 1973, **12**, 1392–1401.
35 R. J. Allen and P. C. Ford, *Inorg. Chem.*, 1972, **11**, 679–685.
36 B. J. Coe and S. J. Glenwright, 2000, **203**, 5–80.
37 T. Jurca, I. Korobkov, G. P. a Yap, S. I. Gorelsky and D. S. Richeson, *Inorg. Chem.*, 2010, **49**, 10635–10641.
38 D. J. Harrison, S. I. Gorelsky, G. M. Lee, I. Korobkov and R. T. Baker, *Organometallics*, 2013, **32**, 12–15.
39 J. a. Montgomery, M. J. Frisch, J. W. Ochterski and G. a. Petersson, *J. Chem. Phys.*, 2000, **112**, 6532.
40 E. D. Glendening, C. R. Landis and F. Weinhold, *J. Comput. Chem.*, 2013, **34**, 1429–1437.
41 H. P. Hratchian and H. B. Schlegel, in *Theory and applications of Computational Chemistry: The First Forty Years*, 2005, pp. 195–249.
42 K. Fukui, *Acc. Chem. Res.*, 1981, **14**, 363–368.
43 E. Cancès, B. Mennucci and J. Tomasi, *J. Chem. Phys.*, 1997, **107**, 3032.
44 P. Hohenberg and W. Kohn, *Phys. Rev.*, 1964, **136**.
45 W. Kohn and L. J. Sham, *Phys. Rev.*, 1965, **140**.
46 A. D. Becke, *J. Chem. Phys.*, 1993, **98**, 5648–5652.
47 C. Lee, W. Yang and R. Parr, *Phys. Rev. B*, 1988, **37**, 785–789.
48 C. G. and J. A. P. M. J. Frisch, G. W. Trucks, H. B. Schlegel, G. E. Scuseria, M. A. Robb, J. R. Cheeseman, J. A. Montgomery Jr., T. Vreven, K. N. Kudin, J. C. Burant, J.M.Millam, S. S. Iyengar, J. Tomasi, V. Barone, B. Mennucci, M. Cossi, G. Scalmani, N. Rega, G. A. Peters, *Gaussian, Inc., Wallingford CT*, 2004.
49 C. Sosa, J. Andzelm, B. C. Elkin, E. Wimmer, K. D. Dobbs and D. A. Dixon, *J. Phys. Chem.*, 1992, 6630–6636.
50 N. Godbout, D. R. Salahub, J. Andzelm and E. Wimmer, *Can. J. Chem.*, 1992, **70**, 560–571.
51 P. N. Clough, B. A. Thrush, And, D. A. Ramsay and J. G. Stamper, *Chem. Phys. Lett.*, 1973, **23**, 7–8.
52 M. E. Jacox and D. E. Milligan, *J. Mol. Spectrosc.*, 1973, 48, 536–559.
53 H. B. E. Jr, G. B. Ellison, H. B. Ellis and G. B. Ellison, *J. Chem. Phys.*, 1983, **78**, 6541–6558.
54 J. Lee and G. B. Richter-Addo, *J. Inorg. Biochem.*, 2004, **98**, 1247–1250.
55 D. Sellmann, T. Gottschalk-gaudig and D. Häuûinger, *Chem. Eur. J*, 2001, **7**, 2099–2103.
56 C. E. Immoos, F. Sulc, P. J. Farmer, K. Czarnecki, D. F. Bocian, A. Levina, J. B. Aitken, R. S. Armstrong and P. A. Lay, *JACS Commun.*, 2005, **127**, 814–815.
57 R. D. Wilson and J. A. Ibers, *Inorg. Chem.*, 1979, **18**, 336–343.
58 J. B. Foresman and Æ. Frisch, *Exploring chemistry with electronic structure methods*, 1996.
59 D. W. Franco, *Coord. Chem. Revews*, 1992, **119**, 199–225.
60 E. C. Constable, in *Metals and Ligands Reactivity*, 1990, pp. 25–48.
61 N. O. Codesido, T. Weyhermüller, J. A. Olabe and L. D. Slep, *Inorg. Chem.*, 2014, **53**, 981–997.
62 V. Shafirovich and S. V. Lymar, *PNAS*, 2002, **99**, 7340–7345.

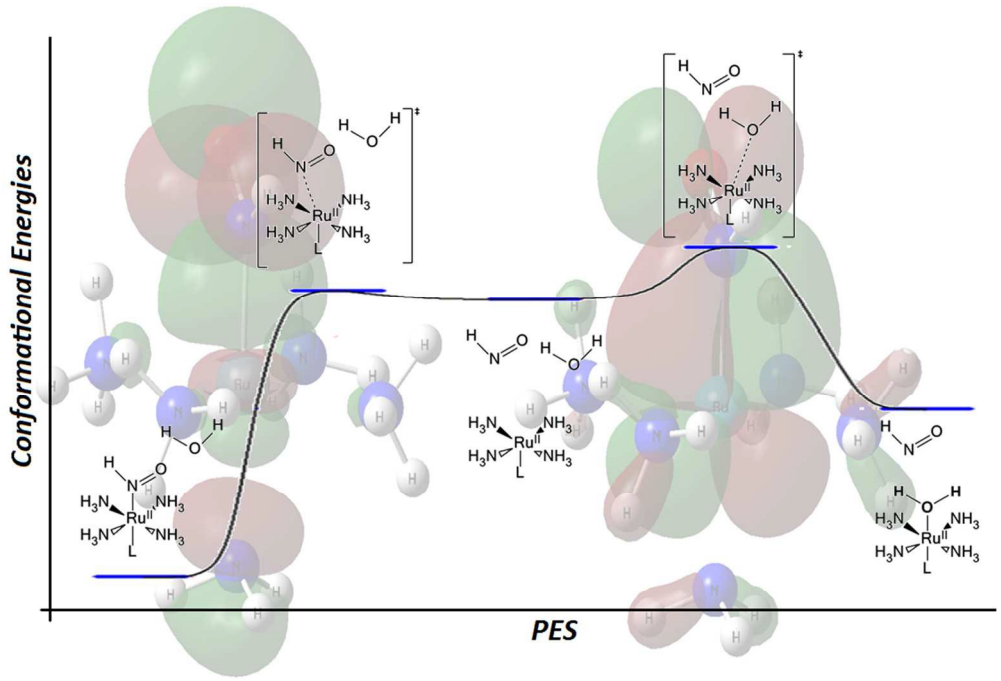

298x204mm (96 x 96 DPI)